A new model to predict Ajisai satellite reflected sunlight flashes and application to the determination of its rotation parameters.

Carlo Calatroni, Gilles Métris, Clément Courde, Duy-Hà Phung, Julien Chabé, Mourad Aimar, Nicolas Maurice, Hervé Mariey

Available online at www.sciencedirect.com

ScienceDirect

Advances in Space Research 75 (2025) 7327–7344

ADVANCES IN SPACE RESEARCH (a COSPAR publication)

www.elsevier.com/locate/asr

A new model to predict Ajisai satellite reflected sunlight flashes and application to the determination of its rotation parameters.

Carlo Calatroni *, Gilles Métris, Clément Courde, Duy-Hà Phung, Julien Chabé, Mourad Aimar, Nicolas Maurice, Hervé Mariey

Observatoire de la Côte d'Azur, Université Côte d'Azur, CNRS, IRD, Géoazur, Campus Azur du CNRS 250 rue Albert Einstein, Valbonne 06250, France

Received 21 November 2024; received in revised form 21 February 2025; accepted 25 February 2025
Available online 28 February 2025

Abstract

In this paper, we propose a model reproducing the sequences of flashes emitted by the Ajisai satellite by reflection of the sunlight on the mirrors all around its surface and received by an observing station. A decisive novelty was added by introducing the curvature of the mirrors, that allows the reconstruction of the observed light curve given the attitude of the satellite. Measurements of the Ajisai's light flux have been acquired using a high frequency (5/10 kHz) linear-detection optical photometry technique from the MéO telescope at Grasse station on the Plateau de Calern site of Observatoire de la Côte d'Azur. A procedure to extract individual flashes from the observed flux and identify the associated mirror on which the reflection occurred has been developed. The analysis of the observed flashes confirmed the validity of the model and allowed us to reconstruct the attitude of the satellite. The satellite rotation has been expressed as a function of the rotation spin axis, the rotation period and the rotation angle around the axis. A method to determine each parameter directly from single pass observations is proposed to fully constrain the satellite attitude using photometry. A precise knowledge of the attitude of the satellite is essential to enable future interesting developments, among others, improving the precision of the synchronization of distant clocks by means of laser links involving Ajisai.

Keywords: Ajisai; Mirrors; Flashes; Linear detection photometry; Satellite rotation

1. Introduction

Ajisai (NORAD 16908, International Designator 1986-061A), also known as EGS, Experimental Geodetic Satellite, is a Japanese geodetic satellite launched by Jaxa (formerly NASDA) on 12 August 1986 (Sasaki and Hashimoto, 1987). The satellite consists in a totally passive GFRP (Glass Fiber Reinforced Plastic) hollow sphere with a mass of 685 kg and a diameter of 2.15 meter (Sasaki and Hashimoto, 1987). No active subsystems, electronics or actuators are present on board. The center of gravity was designed to be within 1 mm from the center of the sphere (Sasaki and Hashimoto, 1987). After launch, it has been placed on a circular orbit with an inclination of 50° at an altitude of about 1500 km and an initial spin rate of about 40 rpm (Sasaki, 1987). A passive nutation dumper keeps the axis of rotation approximately collinear with the axis of symmetry. The direction of rotation has been estimated as clockwise, i.e. opposite to Earth rotation, by Kirchner et al. (2007) using Satellite Laser Ranging (SLR) data. The spacecraft special feature (see Fig. 1), compared to other passive geodetic satellites like LAGEOS, STARLETTE or STELLA, is to be equipped not only with 1436 classical retroreflectors, but also with 318 mirror panels (Sasaki, 1987).

* Corresponding author.
E-mail address: carlo.calatroni@geoazur.unice.fr (C. Calatroni).

https://doi.org/10.1016/j.asr.2025.02.054
0273-1177/

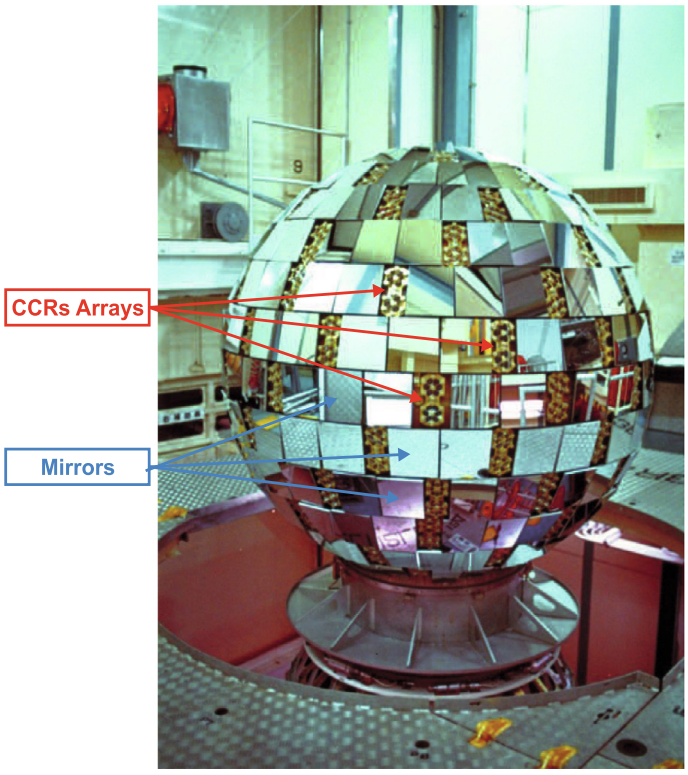

Fig. 1. Ajisai Satellite. (courtesy of JAXA).

While Corner Cube Retroreflectors (CCRs) reflect light in the incident direction and are used for laser ranging, mirrors reflect light in a direction symmetrical to the normal. In this work we use the mirrors to study the satellite rotation. The precise knowledge of the rotation has several interests: (i) this is a good opportunity to assess the validity of theoretical models of the rotation (see e.g. Kucharski et al. (2016)), (ii) the orientation parameters enter in the model of some non-gravitational orbital perturbations, like the Yarkovsky effect (Rubincam, 1988; Sengoku et al., 1995), and (iii) the knowledge of the positioning of the mirrors in space is useful to improve the precision of time transfer by laser link (Kunimori et al., 1992; Liu et al., 2021).

Indeed, time transfer between two SLR stations involves the comparison of the times of flight between each station and the satellite on the one hand and between the two stations via reflection on the satellite on the other. First attempts involving the Grasse and Wettzell stations confirmed that this is technically feasible. To obtain the best accuracy, it is necessary to take into account the relative positions between the different points of reflection on the satellite. To do this, knowledge of the satellite attitude is a key point.

As demonstrated in previous works, photometry using the mirrors and laser ranging using the CCRs both allow to study the rotation parameters. The method using the laser technique relies on the fact that the CCRs reflect the photons not only when they are perfectly aligned with the laser beam (leading to the shortest distance), but also before and after this closest approach; thus the rotation translates into variations of the measured distance at the rotation frequency and its harmonics. Otsubo et al. (2000) demonstrated the possibility to estimate the Ajisai's spin rate by means of the frequency analysis of the laser ranging measurements and evidenced the decrease of the rotation rate over a few hundred days. Kirchner et al. (2007) made an equivalent study using the Graz kHz SLR data. This work was later extended by Kucharski et al. (2009) using 22 years of SLR data, including some at kHz, showing in particular the very similar patterns of the spectra of the rotation period and of the shadow function (which indicates if the satellite is in the Earth's shadow or not). Kucharski et al. (2010a) proposed an empirical model to represent the slow temporal evolution of the spin axis orientation. Kucharski et al. (2016) showed that this measured evolution is consistent with the one predicted by the dynamical models. The laser ranging technique is very interesting since the determination of the rotation parameters is a by-product of measurements that are performed in routine activity for the needs of the International Laser Ranging Service (ILRS) (Pearlman et al., 2019). The photometry of the mirrors, while requiring specific efforts, yields an excellent alternative with perhaps an higher potential.

To our knowledge Otsubo et al. (1998) was the first to use the photometry of the solar light reflected by the mirrors for the determination of the Ajisai's spin rate, to within one mrad/s. Koshkin et al. (2010) extended the method to the determination of the spin axis orientation.

Korobeynikova et al. (2012) used the same kind of technique to estimate the rotation period with an estimated error of 0.1 ms and model its exponential evolution between 2009 and 2010; they also gave a map of the positions of the mirrors on the satellite. Burlak et al. (2014) extended the study between 2009 and 2014 and derived empirical models for the evolutions of the spin axis orientation and the rotation period, and also evidenced additional small quasi-periodic variations of the period, apparently correlated with the crossing of the orbit with the Earth's shadow. The most complete study using the photometric technique is due to Koshkin et al. (2017) who not only determined precession and nutation periods for the evolution of the spin axis orientation and the rotation period compatible with those determined by Kucharski with the laser ranging, but also published an improved (partial) map of the location and orientation of the mirrors.

An extension of the instrumentation of the laser ranging station MéO (Mariey, 2022; Phung et al., 2021) from Côte d'Azur Observatory allows now to monitor the photometric emission from space objects flying over the telescope. This equipment has been used in particular to follow a few passes of Ajisai in 2023 and then, after some improvements, a few passes in 2024. We developed a detailed model capable to reproduce the observed sequence of flashes. In particular, although it is well known and documented that the Ajisai's mirrors are curved, all the previous analyses using the photometric technique assume, explicitly or implicitly, that the mirrors are flat. In the present study, we propose a new model taking into account the curvature of the mirrors and we will compare it with the observations collected at the MéO station. Note that the convex curvature of the Ajisai's mirrors has been modeled in the past allowing for more realistic optical link budget analysis Kucharski et al. (2019) or highly detailed reflectivity mapping of the external surfaces Kucharski et al. (2020). However, to our knowledge, it has not yet been taken into account in determining the rotation parameters. We will show that the curvature of the mirrors radically changes the temporal distribution of the flashes and clearly improves the consistency with the observations, which allows to determine the rotation parameters with confidence.

The paper is organized as follows. In Section 2 we describe the flashes physical model, including the curvature of the mirrors. This model, as well as the parametrization of the Ajisai's rotation, allows to predict the expected sequences of flashes, which are definitively modified by the curvature. In Section 3 we report on the observation of the flashes at the MéO station using linear photometry. In Section 4 we show how the comparison of the model with the observations allows to improve the rotation parameters. Finally, in Section 5 we demonstrate that the optimization of the mirrors installation data, that we do not know a priori with a total confidence, still improves the consistency between the model and observations.

2. Flashes model

2.1. Flash condition

We define $\hat{\mathbf{R}}$ as the opposite of the telescope pointing direction unit vector $\hat{\mathbf{R}} = -\hat{\mathbf{R}}_{Station-Satellite}$, $\hat{\mathbf{S}}$ as a unit vector pointing in the direction of the Sun that can be derived normalizing the Sun position w.r.t. the satellite $\mathbf{s}$ as $\hat{\mathbf{S}} = \frac{\mathbf{s}}{\|\mathbf{s}\|}$.

In principle, if a mirror is specifically oriented, a photon emitted by the Sun in the direction $-\hat{\mathbf{S}}$ is reflected toward the observer in the direction $\hat{\mathbf{R}}$ by a piece of mirror having a normal parallel to the bisector $\hat{\mathbf{B}}$ (Fig. 2), where

$$\hat{\mathbf{B}} = \frac{\hat{\mathbf{R}} + \hat{\mathbf{S}}}{\|\hat{\mathbf{R}} + \hat{\mathbf{S}}\|} \tag{1}$$

We start with a simplified analysis assuming the Sun as a point-like source and flat mirrors (thus with a unique normal for the whole mirror), and we shall introduce more realistic assumptions step by step.

Given the normal $\hat{\mathbf{N}}$ to the flat mirror, we define the symmetric $\hat{\mathbf{R}}'$ of $\hat{\mathbf{R}}$ w.r.t. $\hat{\mathbf{N}}$ as:

$$\hat{\mathbf{R}}' = 2\left(\hat{\mathbf{R}} \cdot \hat{\mathbf{N}}\right)\hat{\mathbf{N}} - \hat{\mathbf{R}} \tag{2}$$

In the case of a point-like Sun of direction $\hat{\mathbf{S}}$, the condition to have a reflection toward $\hat{\mathbf{R}}$, hereafter the "flash condition" is:

$$\hat{\mathbf{R}}' \equiv \hat{\mathbf{S}} \tag{3}$$

Since we are interested only in the photons which are reflected by the external surface of the mirrors, we shall impose:

$$\left(\hat{\mathbf{R}} \cdot \hat{\mathbf{N}}\right) > 0 \tag{4}$$

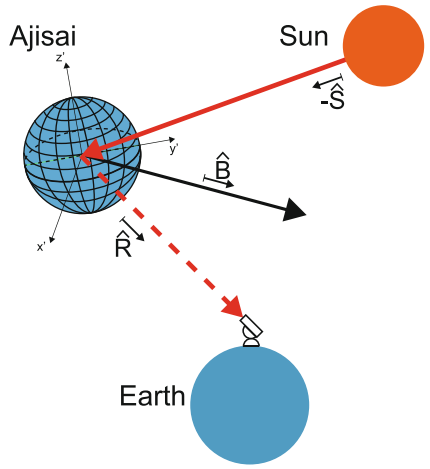

Fig. 2. Earth - Sun - satellite schematic: if a mirror is properly oriented, the sunlight (orange arrow) is reflected towards the station where it is detected by the telescope.

Note that condition $\hat{\mathbf{N}} = \hat{\mathbf{B}}$ is equivalent to condition given by Eq. (3) but the latter is better suited to a generalization to an extended source.

The Sun cannot be considered as a material point but rather as a disk of apparent radius (or angular radius) ε. The flash condition shall be updated accordingly:

$$\angle\left(\hat{\mathbf{R}}', \hat{\mathbf{S}}\right) \leqslant \varepsilon \Rightarrow \ \hat{\mathbf{R}}' \cdot \hat{\mathbf{S}} \geqslant \cos(\varepsilon) \tag{5}$$

Inserting Eq. (2) in Eq. (5), we obtain:

$$2\left(\hat{\mathbf{R}} \cdot \hat{\mathbf{N}}\right)\left(\hat{\mathbf{S}} \cdot \hat{\mathbf{N}}\right) \geqslant \left(\hat{\mathbf{R}} \cdot \hat{\mathbf{S}}\right) + \cos(\varepsilon) \tag{6}$$

The Ajisai satellite mirrors are not flat, as assumed up to now, but curved. This means that each point of the mirror has a different normal and the reflection direction depends on the area of the mirror where it occurs. For this reason, we introduced a discretized model of the mirrors. In order to represent the curvature of an $i-th$ mirror, the mirror is discretized by using a set of unit vectors normal to the surface, $\hat{\mathbf{N}}_{i,j}$, that are evenly distributed over the mirror surface. The mirrors extend over approximately 20 cm, equivalent to an angle of 1.27°, in both dimensions. We used typically a discretization step of 0.1° which is a good compromise between computational cost and fidelity of the model. The mirror's main normal $\hat{\mathbf{N}}_i$, in the center of the mirror, is used as the reference for the discretization.

Now, the flash condition represented by Eqs. (6) and (4) is tested for each of the N^i_{disc} discretized normals $\hat{\mathbf{N}}_{i,j}$. The mirror i is considered as flashing as soon as the condition is verified for at least one normal. We compute the flash indicator

$$\boldsymbol{f}_i = \sum_{j=1}^{N^i_{disc}} \begin{cases} 2\left(\hat{\mathbf{R}} \cdot \hat{\mathbf{N}}_{i,j}\right)\left(\hat{\mathbf{S}} \cdot \hat{\mathbf{N}}_{i,j}\right) \geqslant \left(\hat{\mathbf{R}} \cdot \hat{\mathbf{S}}\right) + \cos(\varepsilon) \\ \left(\hat{\mathbf{R}} \cdot \hat{\mathbf{N}}_{i,j}\right) > 0 \end{cases} \tag{7}$$

Since both the satellite and the Earth are moving and rotating, the flash indicator f_i has to be computed for each desired epoch t_s. An interesting indicator is the proportion of flashing normals compared to the total, tested for each t_s, that gives us an estimate of the flux variation:

$$\boldsymbol{fl}(t_s) = \sum_{i}^{N_{mirrors}} \boldsymbol{fl}_i(t_s) = \sum_{i}^{N_{mirrors}} \boldsymbol{f}_i(t_s)/N^i_{disc} \tag{8}$$

Since at most one mirror is flashing at each $s-th$ time instant, the value of the estimated flux $\boldsymbol{fl}(t_s)$ always lies between 0 and 1.

The computation of the flash condition given by Eq. (7) requires the knowledge, in the same reference frame, of the positions of the Earth station, the satellite and the Sun, as well as of the orientation of the mirrors. The positions of the 3 bodies (Sun, Earth, Ajisai) w.r.t a celestial frame are easily obtained from public ephemeris (Park et al., 2021; Acton et al., 2018; ILRS, 2018). To get the orientation of the mirrors w.r.t the celestial frame one needs (i) their position/orientation in the Ajisai body frame, and (ii) the attitude of Ajisai in the celestial frame. These two topics are addressed in the next sections.

2.2. Mirrors configuration

In the following, the position of a mirror is referenced as the position of its center and its orientation is referenced as the orientation of the normal at the center also called main normal of the mirror. The 318 mirrors are subdivided in 15 rings (labeled $\mathscr{R}_p$ with $p = -7, \cdots, 0, \cdots, +7$), containing between 3 and 27 mirrors having the same latitude ϕ_p. The orientation of the main normal of the mirror corresponds to the orientation of the local normal to the spherical satellite in longitude but can be tilted by an angle τ in latitude (i.e. along the meridian). The mirrors of each ring $\mathscr{R}_p$ could be subdivided in N_p groups of 3 mirrors, hereafter referred to as "triplets" and denoted as $\mathscr{T}_{p,q}$, having the same tilt τ_q, where $q = 1, \cdots, N_p$. As a result, the inclination of the main normal of the mirror w.r.t. the equator is $\Phi_{p,q} = \phi_p + \tau_q$. The 3 mirrors of a given triplet have an irregular distribution in longitude, giving a specific signature to each triplet. The subtle combination of the latitudes of the rings and of the tilts and curvatures of the mirrors leads to a quasi-continuous coverage of the normals in latitude with almost no overlap between the triplets. This ensures that a given station, in night condition, will observe flashes as soon as the satellite is in line of sight and illuminated by the Sun; moreover, the flash observed at a given time comes from a single mirror (see below for more details).

To our knowledge, the table of positions and tilts of the mirrors has not been disclosed by JAXA and it is not available in published literature. However, Korobeynikova et al. (2012) and Koshkin et al. (2017) reconstructed an approximated scheme from photometric observations with CCD technology and the actual result was only partially disclosed through a figure. We reconstructed a scheme of the orientation of the satellite's mirrors from satellite specifications (Sasaki, 1987; Sasaki and Hashimoto, 1987; Hashimoto et al., 2012) and literature data (Korobeynikova et al., 2012; Koshkin et al., 2017). This scheme is partial, in the sense that it does not include high latitudes, but is sufficient to interpret observations performed from our station.

The error resulting from the relative inaccuracy of this scheme constitutes the main potential source of uncertainty in our study but, as this will be shown below, the consistency between our model and our observations indicates that this configuration is globally reliable.

2.3. Ajisai's rotation

Two classical reference frames are used to describe the rotation model: the inertial frame (ICRF) $\mathscr{N} = \left\{\hat{\mathbf{e}}^{\mathscr{N}}_x, \hat{\mathbf{e}}^{\mathscr{N}}_y, \hat{\mathbf{e}}^{\mathscr{N}}_z\right\}$ and the satellite body frame (SBF)

$\mathscr{B} = \left\{\hat{\mathbf{e}}_x^{\mathscr{B}}, \hat{\mathbf{e}}_y^{\mathscr{B}}, \hat{\mathbf{e}}_z^{\mathscr{B}}\right\}$. By ICRF we refer to the International Celestial Reference Frame third major revision ICRF3 (Charlot et al., 2020), an Earth-Centered-Inertial frame. The SBF is here defined as a reference system attached to the body of the S/C, with the origin at its center of mass which is assumed coincident with the geometrical center. $\hat{\mathbf{e}}_z^{\mathscr{B}}$ is collinear to the satellite's axis of symmetry, and $\hat{\mathbf{e}}_x^{\mathscr{B}}$ points towards the centre of one of the 3 mirrors of inclination 0 (thus belonging to the equatorial ring R_0 and with a tilt $\tau = 0$).

As indicated in the introduction, the spin axis $\hat{\mathbf{W}}$ has been assumed collinear with the symmetry axis of the satellite $\hat{\mathbf{e}}_z^{\mathscr{B}}$ as in previous publications (Kucharski et al., 2016; Koshkin et al., 2017).

We define the Ajisai rotation model using an axis-angle representation by means of two quantities: a unit vector $\hat{\mathbf{W}}$ indicating the axis of rotation, and an angle of rotation θ about the axis. We introduce also the corresponding rotation matrix $\left[\mathbf{A}_{B/N}\right]$which transforms the same physical vector between the ICRF and the SBF. For example, the transformation applied to the normal $\mathbf{n}_i$ associated to the mirror i reads

$$\mathbf{n}_{\mathscr{B},i} = \left[\mathbf{A}_{B/N}\right] \cdot \mathbf{n}_{\mathscr{N},i}, \tag{9}$$

and conversely

$$\mathbf{n}_{\mathscr{N},i} = \left[\mathbf{A}_{B/N}^T\right] \cdot \mathbf{n}_{\mathscr{B},i} \tag{10}$$

where $\left[\mathbf{A}_{B/N}^T\right]$ is the transpose of $\left[\mathbf{A}_{B/N}\right]$.

The $\left[\mathbf{A}_{B/N}\right]$ matrix can be rewritten as a sequence of the two rotation matrices:

$$\left[\mathbf{A}_{B/N}\right] = \left[\mathbf{A}_3(\theta)\right] \cdot \left[\mathbf{A}_{rod}^{\hat{\mathbf{z}}\mapsto\hat{\mathbf{W}}}(\hat{\mathbf{u}}, \psi)\right]. \tag{11}$$

The rotation matrix $\left[\mathbf{A}_{rod}^{\hat{\mathbf{z}}\mapsto\hat{\mathbf{W}}}\right]$ aligns the z-axis of the new reference frame with the spin axis $\hat{\mathbf{W}}$, such as $\hat{\mathbf{e}}_z^{\mathscr{B}} = \hat{\mathbf{W}}$. This transformation can be expressed as a rotation of angle

$$\psi = acos\left(\hat{\mathbf{e}}_z^{\mathscr{N}} \cdot \hat{\mathbf{W}}\right) \tag{12}$$

around an axis $\hat{\mathbf{u}}$ orthogonal to $\hat{\mathbf{W}}$ and to $\hat{\mathbf{e}}_z^{\mathscr{N}}$:

$$\hat{\mathbf{u}} = \frac{\hat{\mathbf{e}}_z^{\mathscr{N}} \wedge \hat{\mathbf{W}}}{\|\hat{\mathbf{e}}_z^{\mathscr{N}} \wedge \hat{\mathbf{W}}\|} \tag{13}$$

It can be expressed as (using e.g. the Rodrigues formula):

$$\left[\mathbf{A}_{rod}^{\hat{\mathbf{z}}\mapsto\hat{\mathbf{W}}}(\hat{\mathbf{u}}, \psi)\right] = \begin{bmatrix} c + (1-c)u_x^2 & (1-c)u_x u_y - su_z & (1-c)u_x u_z + su_y \\ (1-c)u_x u_y + su_z & c + (1-c)u_y^2 & (1-c)u_y u_z - su_x \\ (1-c)u_x u_z - su_y & (1-c)u_y u_z + su_x & c + (1-c)u_z^2 \end{bmatrix} \tag{14}$$

with $c = \cos(\psi), s = \sin(\psi)$.

Then $[\mathbf{A}_3(\theta)]$ is the rotation matrix of angle θ about $\hat{\mathbf{e}}_z$:

$$[\mathbf{A}_3(\theta)] = \begin{bmatrix} \cos(\theta) & \sin(\theta) & 0 \\ -\sin(\theta) & \cos(\theta) & 0 \\ 0 & 0 & 1 \end{bmatrix}. \tag{15}$$

The rotation angle θ is time dependent and we assume, as previous authors, that it can be reasonably expressed, on a short time of less than one hour, as:

$$\theta(t) = \theta_0 + \dot{\theta} \cdot (t - t_0) \tag{16}$$

where $\dot{\theta}$ is the angular velocity which can be expressed as a function of the satellite rotation period T according to

$$\dot{\theta} = \frac{360}{T}\ [deg], \tag{17}$$

and θ_0 is the value of θ at a conventional initial epoch t_0.

Finally:

$$\left[\mathbf{A}_{B/N}\right] = \left[\mathbf{A}_{B/N}\right]\left(\hat{\mathbf{W}}, T, \theta_0, t\right) \tag{18}$$

The spin axis and the rotation period are time-varying. Empirical models of their evolutions are available in the literature. According to Kucharski et al. (2016), the spin axis direction evolution is represented using a precession-nutation model. The precession cone period is close to 35.6 years and is defined counterclockwise while the nutation cone period is close to 117 days and is defined clockwise. Various authors (Kirchner et al., 2007; Kucharski et al., 2009; Kucharski et al., 2010b; Kucharski et al., 2016; Korobeynikova et al., 2012; Koshkin et al., 2017) have represented the rotation period evolution as an increasing exponential, all the models being close to each other. For example, Koshkin et al. (2017) gives:

$$T(t) = 1.4934 \cdot \exp\left(0.000040553 \cdot (t - t_0)\right) \tag{19}$$

where t and t_0 are in days and t_0 is the Ajisai launch date (12/08/1986, Modified Julian Days 46654), and T is obtained in s.

The above representations justify to assume constant values for the spin axis and the rotation period during a single pass of Ajisai above a given station. Indeed, during these 20 min at most, the direction of the spin axis changes by less than $2 \cdot 10^{-3}$ deg while the rotation period varies less than $2 \cdot 10^{-6}$ s. The above models are used to compute starting values of the spin axis direction and of the rotation period at the epoch of the pass (e.g. at the time of the first observation). Then, an optimization process will lead to a correction of these parameters (see below). To do this we adopt a representation of the direction of the spin axis in spherical coordinates: the right ascension α and the declination δ.

We end up with

$$\left[\mathbf{A}_{B/N}\right](t) = \left[\mathbf{A}_{B/N}\right](t, \alpha, \delta, T, \theta_0) \tag{20}$$

Finally, the transformation depends on the four parameters $\alpha, \delta, T, \theta_0$.

2.4. Expected flashes sequences

As explained in Section 2.2, the combination of the positions, tilts and curvatures of the mirrors leads to the fact that, whatever is the considered angle w.r.t. the satellite equator, there are always some parts of some mirrors having an inclination corresponding to this angle. Due to the non-regular distribution of the mirrors, the satellite rotation around the spin axis generates a specific sequence of flashes which is dependent on the orientation of the spin axis.

The delays between the successive flashes due to the triplet depend on the separation of the mirrors in longitude and on the rotation period (Fig. 3):

$$\delta t_{a,b}\left(\mathscr{T}_{p,q}\right) = \frac{T \cdot \left(\lambda_b\left(\mathscr{T}_{p,q}\right) - \lambda_a\left(\mathscr{T}_{p,q}\right)\right)}{360} \tag{21}$$

where a and b designate two successive mirrors of the triplet $\mathscr{T}_{p,q}$ and λ_a and λ_b are their respective longitudes in degrees.

Fig. 4 shows an example of the sequence of flashes which should be observed from the MéO station according to our model, during one pass of Ajisai. The model uses as input: the orientation of the spin axis issued from the nutation precession model of Kucharski et al. (2016), the value of the rotation period computed according to Eq. (19) and $\theta_0 = 0$ for the initial rotation angle at t_0. The top panel of the figure uses flat mirrors whereas the two following panels are produced with the more realistic curved mirrors. There are two important modifications due to the curvature: (i) contrary to the flat mirrors case, there is no interruption in the sequence of flashes, and (ii) adjacent triplets are separated by a transition characterized by the occurrence of up to 6 flashes (of smaller intensity) per rotation period, corresponding to the partial illumination of the 2 adjacent triplets by the Sun which is not a point-like source. Note that these transitions do not occur with flat mirrors because the difference of inclination between two adjacent triplets (1.27 deg.) is larger than the apparent diameter of the Sun (about 0.5 deg.). The lowest panel represents the flashes as a function of the inclination of the reflecting mirror. This highlights the transitions between two adjacent triplets.

3. Photometry at MéO station

The MéO (Metrology and Optics) station, generally known as "Grasse Station" and referred in the ILRS networks as GRSM 7845 was initially designed in the framework of a laser ranging program dedicated to the Moon, known as Lunar Laser Ranging (LLR). It subsequently enlarged its scientific objectives to laser links in general, including satellite laser ranging (SLR), and participates to the ILRS network and to various other research activities. For example, the station is also equipped with a photometry package which, added to the tracking system commonly used for SLR, allows to observe and detect the Ajisai's flashes during its pass above the station.

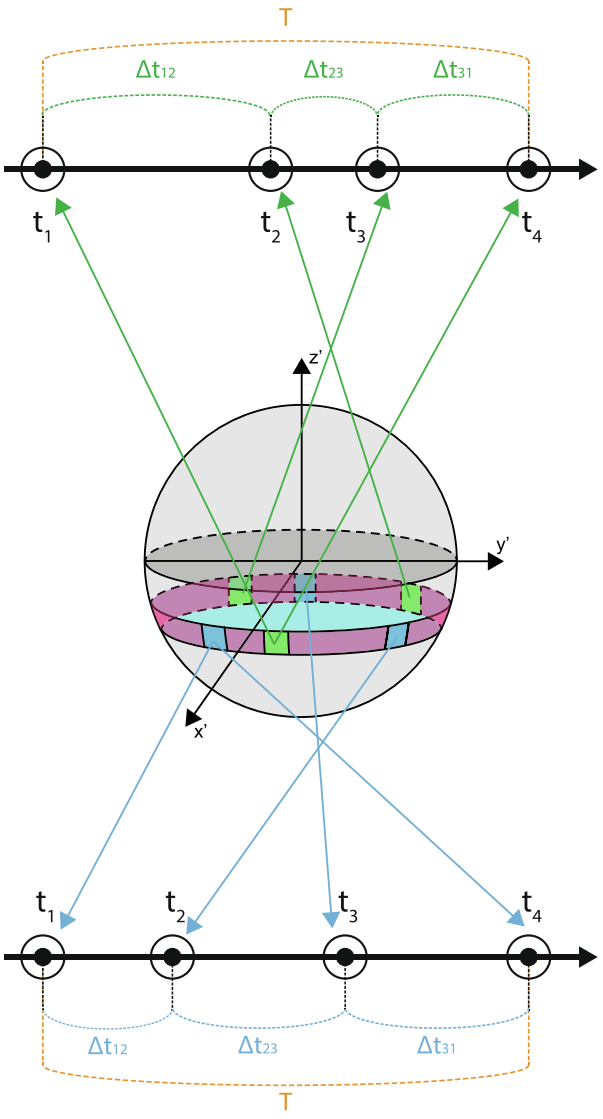

Fig. 3. The mirrors are distributed on different rings with different latitudes as visible on Fig. 1. Moreover, on a given ring (in pink on this figure) the mirrors are subdivided in "triplets", groups of 3 mirrors that have the same tilt: thus two triplets of the same ring have the same latitude but different tilts, and consequently different inclinations w.r.t. the spin axis. Due to the mirrors curvature, each triplet is physically associated to an "inclination band". The figure shows only two triplets for clarity but the ring is covered with adjacent mirrors. As a consequence of the satellite movement and the Earth's rotation, the triplet responsible for the reflection viewed from a given station, changes during the pass of the satellite. Due to the rotation of the satellite around its spin axis, three flashes (one by each of the 3 mirrors) per revolution are generated. The distribution of the mirrors in longitude, specific to each triplet, leads to a specific sequence of delays between the flashes allowing the identification of the triplet. Additionally the delay between two successive flashes generated by the same mirror gives directly the apparent .rotation period.

3.1. Instrumentation

The station is equipped with a 1.54 meter Ritchey Chretien telescope installed on an Alt-Az mount and controlled by a computer. The optical flux from Ajisai is collected by MéO telescope. The telescope tracks the direction of the

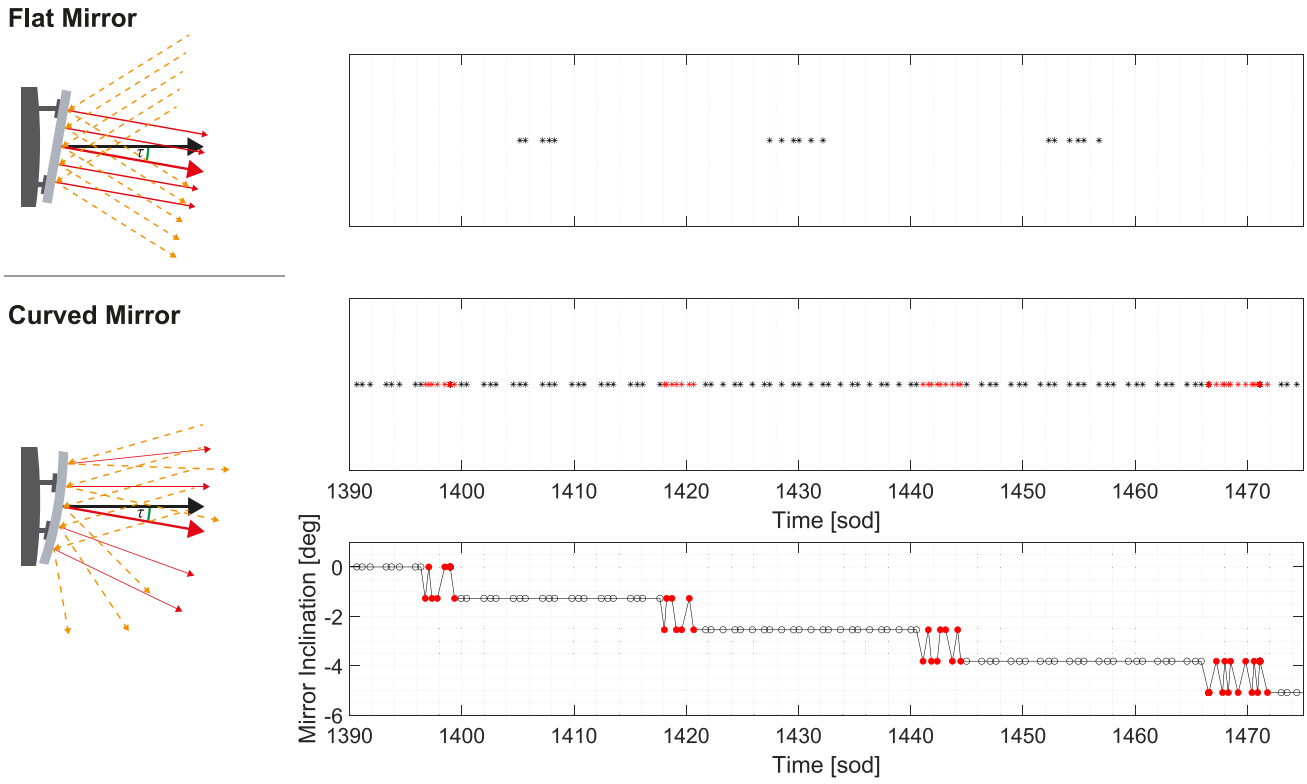

Fig. 4. Comparison of the sequences of flashes simulated with a model using flat mirrors (top panel) and with a model using curved mirrors (middle panel). The curvature of the mirrors leads to many additional flashes and also to transitions. As illustrated on the lower panel, during the transitions two adjacent triplets can be seen from the station, leading to the reception of more than three flashes in a rotation period; the corresponding points are in red on the middle and lower panels.

moving target using precise pass predictions and a tracking camera. The optical spot is maintained at the center of the photo-detector thanks to an auto-tracking performed by a TipTilt mirror and a high-speed camera with a field of view of ~ 20 arc seconds. The active zone of the photo-detector is 1.2 mm diameter, which corresponds to a FoV of 25 arcsec (or 120 μrad) when combining with the 10 m effective focal length of receiving telescope. Its size covers completely the spot size of incoming optical flux, $\sim 2-3$ arcsec FWHM (Full Width at Half Maximum) dominated by the atmospheric turbulence. Actually, the digitizing system consists of a low-cost, portable, digitizer which is combined with a high-sensitivity photo-detector. The entire acquisition chain has a bandwidth of 2 kHz. A photo-detector with a 2 kHz bandwidth, compatible with Ajisai's flash duration (which is about 10 ms), is used to provide a linear measurement of the received sunlight photon flux. The electrical output of the photo-detector is sent to a digitizer in order to record the flux variation at high sampling rate ($>$ 5 kHz) in continuous mode. Each sample is digitized with 23 bits. Two experiments, producing data at 5 and 10 ksamples per second respectively, were carried out on Ajisai. The whole system is installed at the Nasmyth of MéO telescope and operated via Ethernet from the control room. The external 10 kHz clock rectangular signal is generated from a 10 MHz signal coming from the Time and Frequency Lab equipped with an atomic clock. The frequency error of the 10 MHz signal is smaller than 10^{-14} and the timing jitter of the PPS signal is smaller than 100 ps. The external controlling mode of the digitizer allows us to determine the starting time of data recording with a worst case error smaller than 5μs RMS.

3.2. Observations and preprocessing

Raw observations data consist of linearly detected light flux measurements at equispaced time instants. In order to effectively extract useful information, it is necessary to preprocess the raw data to detect flashes. First, it is necessary to identify the time windows in which there is actually a reflection, distinguishing flashes from the background noise. We then enrich the data with the information needed for certain stages of the analysis: firstly, we associate a single epoch (the middle of the window containing the flash) with each identified flash and, secondly, we identify the mirror responsible for the reflection.

The first step of the preprocessing is the identification of the flash time windows. In the absence of flash, the observed flux is mainly generated by the diffuse reflection of sunlight on the satellite's sphere, direct light from the stars (and more rarely from the Moon) entering the field of view, and stray light from the station's surroundings.

The detected flux grows and decreases rapidly respectively at the beginning and at the end of a flash time window while there is a plateau between (Fig. 5). As seen in the figure, this behavior is clearly distinguishable and the simple application of a well chosen threshold is very efficient to select the data corresponding to the sunlight reflected by the mirrors.

To further process the observations and the sequence of flashes, we need to associate a single nominal epoch to each flash. The midpoint of the flash in terms of time duration is used as the reference epoch and only this epoch is maintained in the processed light curve. It is necessary to set certain conditions such as the duration of a flash (imposed conservatively between 4 and 15 ms in our case).

As expected from modeling, there are some time windows during which the received reflected light progressively shifts from one inclination band to another. During these transition time windows, two triplets of mirrors are flashing in the course of a single rotation period. Even if the model predicts these transitions, we decided, for the time being, to disregard these flashes in order to simplify the subsequent analyses. These are easily detected by testing if, for a given flash, there are more than three other flashes in the next rotation period.

Note that, additionally to the flashes of high intensity corresponding to the reflection on the mirrors, we also observe flashes of smaller intensity, even out of the transition zones. We verified that the time distribution is fully consistent with the positions of the CCRs panels. The detailed analysis is more complex than for the mirrors, since both the surfaces of the CCRs, as was observed for LAGEOS (Currie et al., 1997), and of their supports can be involved, depending on the angle of incidence. This work is in progress.

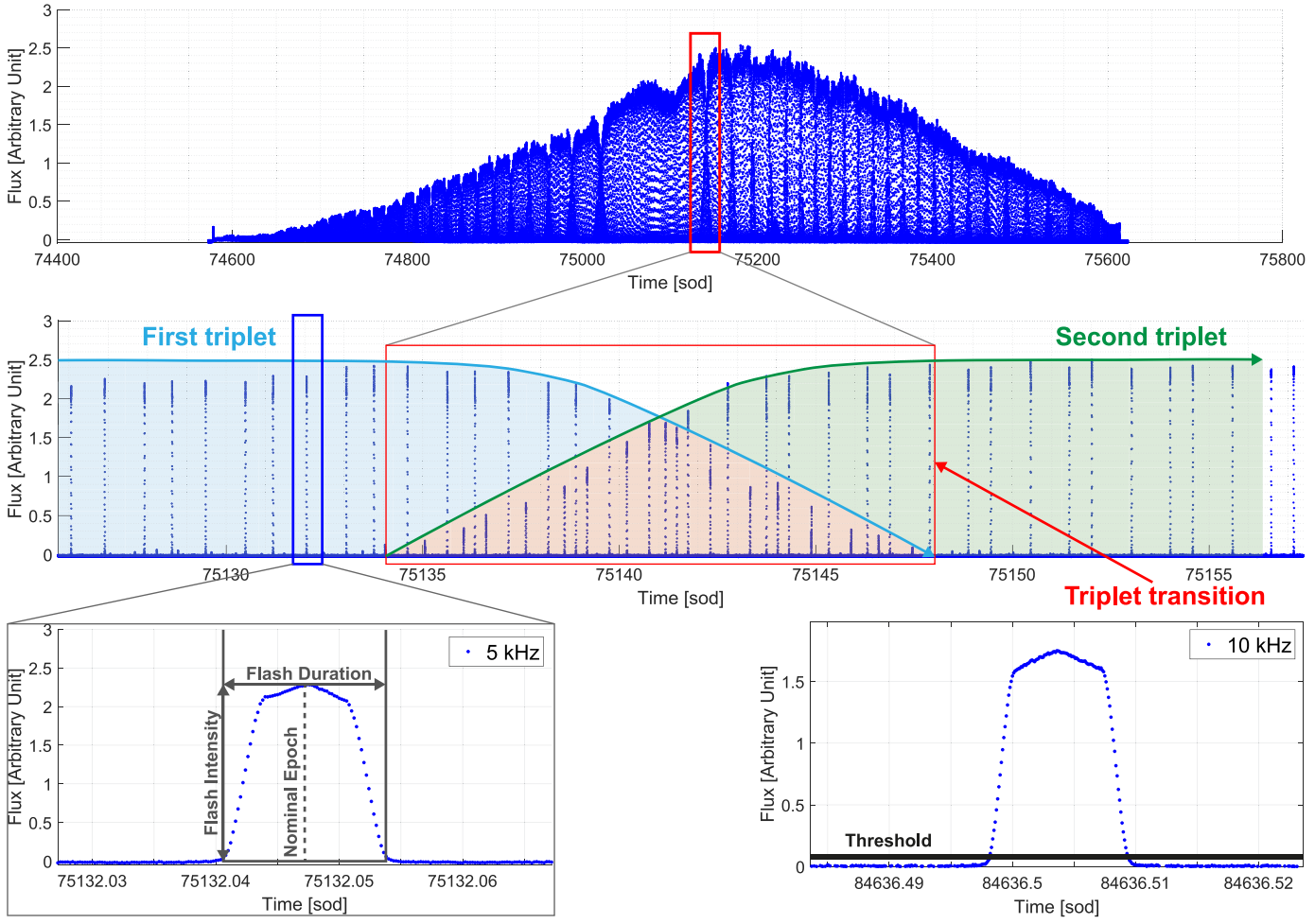

Fig. 5. Measurement of the optical flux using linear photometry at a sampling rate of 5 kHz during a pass of the Ajisai satellite above the MéO station on 26/04/2023. By viewing the data of the entire pass (top panel), we can see that there are fluctuations in the flux intensity and that the flux decreasing and increasing zones are overlapped at the edges. The zoom (middle panel) shows that these are definitely the transitions that we predicted in the model. We can clearly see three flashes for each rotation before (blue background) and after (green background) and up to 6 flashes during the transition (red background). The bottom left panel depicts in detail a flash with a monitoring at 5 kHz; it can be compared with a flash from another pass observed at 10 kHz (bottom right panel). In this last panel, note the threshold applied to distinguish the reflected flux from the noise.

3.3. Comparing observations and model with a priori rotation parameters

The model developed in Section 2 allows to compute the instants of reflection of the sunlight on the satellite while the station records the times of reception of the flashes. It would be possible (and, in a way, more natural) to compute these times of reception from the model. But, since one of our goals is to improve the rotation parameters of the satellite, we preferred to work at the satellite level and first deduce the emission date $t_{reflection}$ of the flashes from their recorded reception date $t_{reception}$:

$$t_{reflection} = t_{reception} - \frac{d_{Station-Satellite}}{c} \tag{22}$$

The propagation of light from the satellite to the station does not take place entirely in vacuum but partially in the atmosphere. However, from a rough estimate, the additional contribution to time delay due to the atmosphere does not exceed 10^{-5} s and is therefore totally negligible. The atmosphere also introduces a refraction related to the satellite's apparent elevation above the horizon, which, however, does not exceed 0.1 deg at 10 deg elevation and cancels exponentially as it approaches the zenith, and is therefore also negligible in our scenario.

The model predicts not only the epochs of flashes but also which mirror is at the origin of each flash. For a full comparison we have to equivalently identify the mirror that reflected the sunlight for each observed flash. This is achievable thanks to the non-regular distribution of the mirrors, leading to a unique signature in terms of the delay between the successive flashes of each triplet, which allows to identify, first the triplet, and then the mirror on which the reflection occurred. Fig. 6 shows an example of a comparison of observed and modeled sequences of flashes. In this case, the model uses a priori values of the rotation parameters, i.e. from empirical predictions from Kucharski et al. (2016) and Koshkin et al. (2017).

We can notice an interesting similarity between the two curves, both in terms of flashes sequences as function of time and in terms of inclination of the reflecting mirrors. This confirms that a model that includes the curvature of the mirrors can give a satisfactory account of what is observed. However, the coincidence is not perfect.

To go beyond this qualitative comparison, we introduce a quantitative criteria using the full rate observations rather than a single instant for each flash. We adopt the time sampling of the photometric observations (5 kHz for the old ones and 10 kHz for the recent ones) and for each point i we associate an index f_i which is set to 1 if the reflected sunlight is received by the telescope and to 0 otherwise. The sets of indices are generated both from the photometric observations (noted f_i^o) and from the results of the simulations using the model (noted f_i^m). Thus, we can compare the two sets of indices to measure the consistency between the observations and the model. In principle, we should compute the model prediction for all observed samples of the pass, i.e. for about 15 x 60 s x 10^4 Hz $= 9 \cdot 10^6$ time samples for a typical pass. To reduce the computational cost, we consider only the time instants for which there is a detection in the observations and we check if the model also predicts a flash; since only 3 flashes of about 10 ms occur during each rotation of about 2.6 s, the number of samples tested with the model is typically reduced by a factor 100. We define the ratio of matching points, ranging between 0 and 1

$$M = 1 - \frac{1}{n_s}\sum_{l=1}^{n_s}\left(f_l^o \cdot \left(f_l^o - f_l^m\right)\right) \tag{23}$$

where n_s is the number of observed flashing points for the pass. Note that this matching ratio is very sensitive to the quality of the prediction since there is a very large number of tested points and an offset of a few ms in the prediction of the flashes sharply decreases M or even cancels it if the offset exceeds the duration of the flash, i.e. 10 ms or a little more. For example, using the a priori rotation parameters in the model, M was equal to 0 for all the passes. This does not mean that the rotation parameters are strongly false but rather that the quality of the observations and the sensitivity of the criteria makes it possible to improve (or more modestly to update, since they result from an extrapolation over a long duration) these parameters.

4. Optimization of the rotation parameters

4.1. General strategy

In the following, we use the observations to improve the knowledge of the rotation parameters. By rotation parameters we mean the unit spin axis orientation parametrized by its right ascension and its declination, the rotation period and the initial rotation angle (see Section 2.3).

The estimation of the rotation parameters is achieved in two steps. A first set is determined from the sequences of flashes, that was subsequently enriched with the identification of the mirrors associated with the flashes. The parameters are computed directly from the data derived from the preprocessing (epoch of the flash, inclination and longitude of the identified mirror) without using the more sophisticated simulations explained in Section 2. For this step the parameters are estimated sequentially: first, the spin axis is determined, then the apparent rotation period which is corrected to get the "true" or "sidereal" period, and finally the initial rotation angle at the nominal initial instant of the pass is estimated. This direct determination is very fast but the curvature of the mirrors is neglected by considering only the main normal to the mirrors and the Sun is considered as point like. In a second step the direct determination serves as a starting point for a global optimization aiming at bringing the simulated flashes (with the full model) closer to the observed ones by adjusting all the parameters simultaneously. This method includes the effect of the extended Sun and of the mirror curvature and refines the

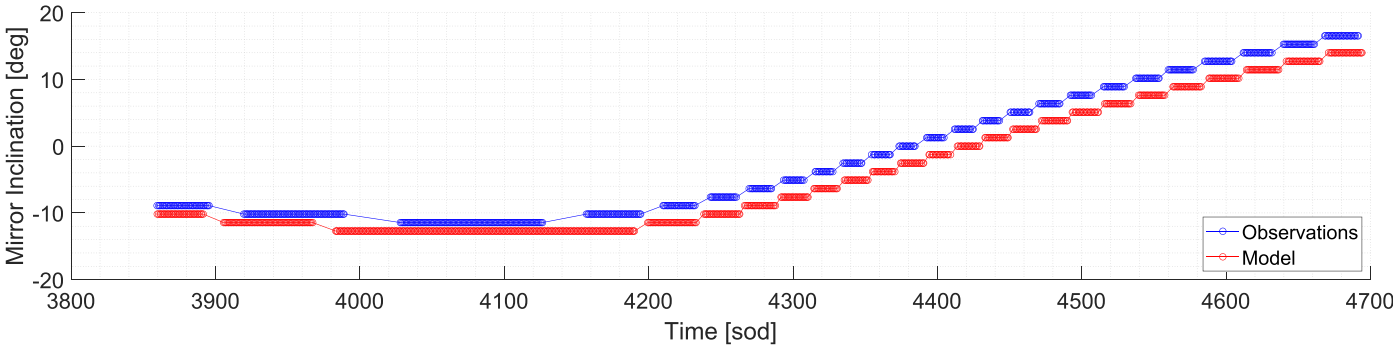

Fig. 6. Comparison of sequences of flashes derived from observations (in blue) and from the model (in red) with a priori rotation parameters, for a pass of Ajisai above the MéO station on 20/04/2023. Flashes during transitions have been discarded.

results of the direct approach but is more time consuming. Combining the two methods, we obtain a high accuracy in the results with a reasonable computational cost.

4.2. Direct determination of the spin axis

As explained in Section 2.1, with the simplified model in which the curvature of the mirrors and the size of the Sun are neglected, the light emitted by the Sun in direction $\hat{\mathbf{S}}$ is reflected towards the satellite-telescope direction $\hat{\mathbf{R}}$ by a mirror of normal $\hat{\mathbf{N}}$ if and only if

$$\hat{\mathbf{N}} = \frac{\hat{\mathbf{R}} + \hat{\mathbf{S}}}{\|\hat{\mathbf{R}} + \hat{\mathbf{S}}\|} = \hat{\mathbf{B}} \tag{24}$$

Since the bisector $\hat{\mathbf{B}}$ is known with an excellent precision from the Sun's, Earth's, and Ajisai's ephemeris, this allows to compute $\hat{\mathbf{N}}$. In particular, the above relation can be projected on the spin axis $\hat{\mathbf{W}}$:

$$\hat{\mathbf{N}} \cdot \hat{\mathbf{W}} = \hat{\mathbf{B}} \cdot \hat{\mathbf{W}} \tag{25}$$

which can be rewritten as

$$\cos\Phi = \cos\beta \tag{26}$$

where Φ is the inclination of the identified normal and β is the latitude, in the satellite frame, associated to $\hat{\mathbf{B}}$.

The potential discrepancy between β and Φ can be interpreted as a misorientation of the spin axis. That is why the objective will be to search for the spin axis orientation which minimizes the discrepancy. The method is inspired by what was proposed in Burlak et al. (2014) and later in Koshkin et al. (2017).

In fact, the relation Eq. (26) cannot be perfectly satisfied for several reasons: simplifications in the model, observational errors and uncertainty of the inclination of the mirrors. That is why, in practice, we shall minimize the cost function

$$F_{\text{spin}}(\alpha,\delta) = \sum_{k=1}^{N_{flash}} [\Phi_k - \beta_k(\alpha,\delta)]^2 \tag{27}$$

where the summation includes all the selected flashes of the pass.

Fig. 7 shows the results of the spin axis determination for two groups of passes. Passes in the first group (in red) were observed between 19 April and 2 May 2023 at a sampling frequency of 5 kHz, while Passes in the second group (in blue) were observed between 16 and 22 June 2024 at a sampling frequency of 10 kHz. The fact that the points are close to each other inside each group covering short periods (14 days for the red group and 6 days for the blue group) confirms the hypothesis of a slow evolution on the one hand and the consistency of the results on the other. On the contrary, there is a clear evolution between the two groups separated by more than one year.

The estimation process does not provide the accuracy associated to the determination of the spin axis. Nevertheless the comparison of spin axis orientations obtained from two close passes allows to estimate the consistency. For

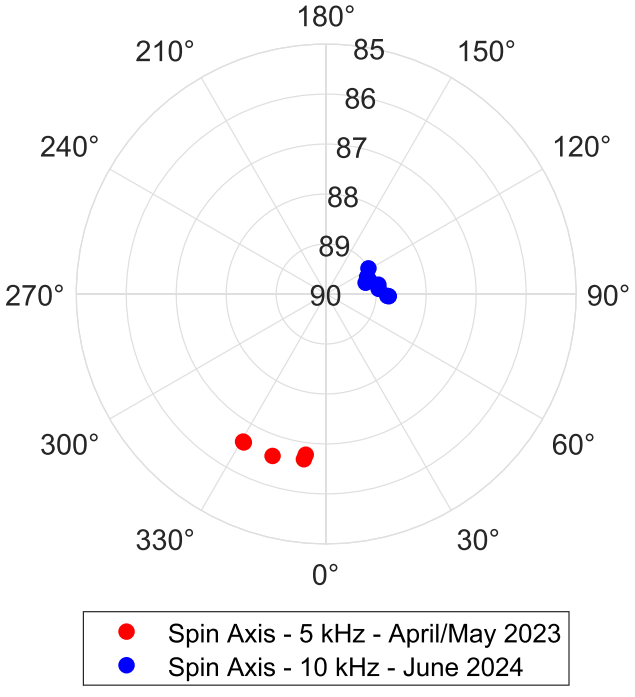

Fig. 7. Spin axis optimization results. Two groups of points are clearly visible: the first (red) is associated to 5 kHz observations taken in April/May 2023 while the second group (blue) is associated to 10 kHz measurements taken in June 2024.

example, if we consider the 4 pairs of passes observed in June 2024, the two successive passes of each pair are typically separated by 2 h and, according to the Kucharski model of evolution, the corresponding displacement of the spin axis direction is expected to be smaller than 0.01 deg. Comparatively, the difference between our corresponding estimates ranges between 0.03 and 0.25 deg. Thus we can assume that these differences are mainly due to estimation errors rather than to a real motion. Thus we adopt 0.25 deg. as a conservative value of the error associated to the spin axis determination, that is probably pessimistic.

4.3. Direct determination of the rotation period

The rotation period represents the time needed by the satellite to complete one entire rotation around the spin axis $\hat{\mathbf{W}}$. The "apparent" or "synodic" rotation period is the value of the rotation period as it is seen from an observer, i.e. the station. To get the "true" or "sidereal" period, we need to apply corrections to take into account the motion of the observer.

If we consider that in each period exactly 3 flashes are present (which should be the case since the transitions have been suppressed during the preprocessing), it is clear that it is sufficient to know the epochs of 4 successive flashes belonging to the same triplet (i.e. having the same inclination in the body frame) to obtain the apparent rotation period of the satellite (illustrated on Fig. 3). This method will be referenced as the "4 flashes method" in the following.

More precisely, given a selection of four successive flashes identified by indices k_1, k_2, k_3 and k_4, the first and the fourth flashes are generated by the same mirror and the rotation period T' can be easily computed as:

$$T' = t(k_4) - t(k_1) \tag{28}$$

From an implementation point of view, the most critical step is the selection of the 4 successive flashes, generated by the same triplet of mirrors, in the correct sequence (i.e. all the flashes in the sequence must be present), so that the first and fourth flashes must be associated with the same mirror. The method consists in: dividing the preprocessed flash epochs into groups generated by the same triplet of mirrors and consequently with the same inclination, selecting for each flash other 3 adjacent flashes, calculating the period according to Eq. (28) and finally removing wrongly computed values due to missing flashes.

The sidereal rotation period T corresponds to the time it takes for any point of the satellite (represented by a normal unit vector in our case) to make a rotation around the spin axis and return to its initial position with respect to an inertial reference frame centered on the satellite:

$$\hat{\mathbf{N}}(t+T) = \hat{\mathbf{N}}(t) \;\Rightarrow\; \hat{\mathbf{N}}(t+T) - \hat{\mathbf{N}}(t) = \mathbf{0} \tag{29}$$

However, with the 4 flashes method explained above, we determine the period T' separating two consecutive alignments of the normal with the bisector $\hat{\mathbf{B}}$:

$$\hat{\mathbf{N}}(t) = \hat{\mathbf{B}}(t) \quad \text{and} \quad \hat{\mathbf{N}}(t+T') = \hat{\mathbf{B}}(t+T') \tag{30}$$

which leads to

$$\hat{\mathbf{N}}(t+T') - \hat{\mathbf{N}}(t) = \hat{\mathbf{B}}(t+T') - \hat{\mathbf{B}}(t) \tag{31}$$

The comparison of Eqs. (29) and (30) shows that the apparent (synodic) period T' differs from the real (sidereal) period T. In other words, T' must be corrected from the variation of $\hat{\mathbf{B}}$ in the inertial frame. Eq. (30) can be shorten into

$$\Delta\hat{\mathbf{N}} = \Delta\hat{\mathbf{B}} \tag{32}$$

Now the point is to convert the variation $\Delta\hat{\mathbf{N}}$ into a correction ΔT of the rotation period. First, Eq. (A.7) shows how to interpret $\Delta\hat{\mathbf{N}}$ in terms of modification of the spherical coordinates and in particular of $\Delta\lambda$:

$$\Delta\lambda = \frac{1}{\cos^2\Phi}\Delta\hat{\mathbf{N}} \cdot \left(\hat{\mathbf{W}} \wedge \hat{\mathbf{N}}\right) \tag{33}$$

According to Eqs. (30) and (32), this is equivalent to:

$$\Delta\lambda = \frac{1}{\cos^2\beta}\Delta\hat{\mathbf{B}} \cdot \left(\hat{\mathbf{W}} \wedge \hat{\mathbf{B}}\right) \tag{34}$$

where $\Delta\hat{\mathbf{B}} = \hat{\mathbf{B}}(k_4) - \hat{\mathbf{B}}(k_1)$, and

$$\cos^2\beta = 1 - \left(\hat{\mathbf{W}} \cdot \hat{\mathbf{B}}\right)^2 \tag{35}$$

Now $\Delta\lambda$ can be converted into a correction of period using the simple relation

$$\Delta T = \frac{\Delta\lambda}{2\pi}T' = \frac{T'}{2\pi\cos^2\beta}\Delta\hat{\mathbf{B}} \cdot \left(\hat{\mathbf{W}} \wedge \hat{\mathbf{B}}\right) \tag{36}$$

The sidereal rotation period T writes

$$T = T' + \Delta T. \tag{37}$$

A value $T^{(g)}$ of the sidereal rotation period can be computed according to the above procedure for each set g of four successive flashes of the pass. Finally, the sidereal rotation period T_{pass} is calculated by averaging all the N_T corrected values $T^{(g)}$ of the pass:

$$T_{pass} = \frac{1}{N_T}\sum_{g=1}^{N_T} T^{(g)} \tag{38}$$

Fig. 8 shows an example of raw (red points) and corrected (blue points) values of the rotation period determined from a pass observed in 2023. The correction clearly improves the consistency of the different estimates. Despite this excellent consistency, there is a remaining pattern (pieces of parallel curves) related to the sampling (0.2 ms in this case).

The RMS of the residuals w.r.t. the mean is around 10^{-4} s. Since there are typically more than 500 individual values in a pass, the standard error of the mean $\sigma_{T_{pass}}$ associated to the sidereal rotation period T_{pass} is smaller than 10^{-5} s (Table 1).

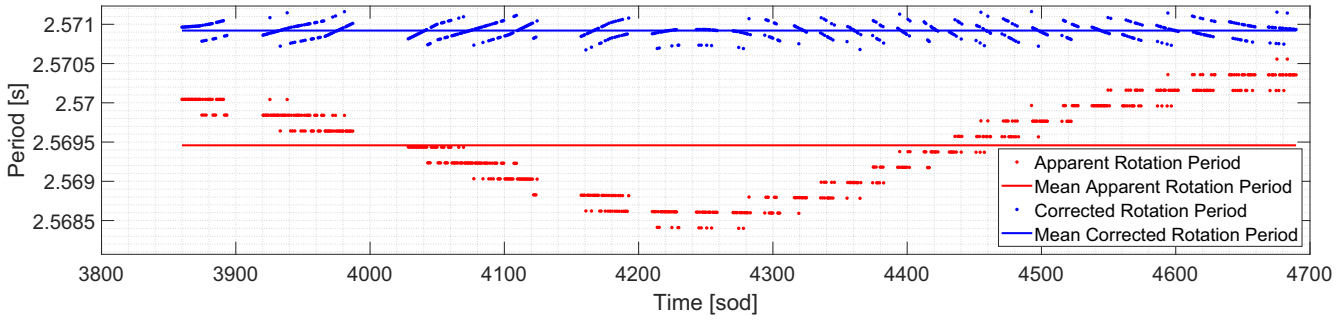

Fig. 8. Example of determination of rotation period using the 4-Flashes Method for an Ajisai pass observed on 20/04/2023.

Table 1
Sidereal rotation period T_{pass} and associated standard error $\sigma_{T_{pass}}$ for 13 passes observed at 5 and 10 kHz sampling rate (see the text for more details).

Pass Identifier	Epoch [MJD]	Sampling Rate	$T_{pass}[s]$	$\sigma_{T_{pass}}$ $10^{-6}[s]$
19/04/2023_1	60053.964	5 kHz	2.570910	4.3
20/04/2023_1	60054.049	5 kHz	2.570921	3.7
26/04/2023_1	60060.869	5 kHz	2.570640	4.4
02/05/2023_1	60066.813	5 kHz	2.570980	8.5
02/05/2023_2	60066.897	5 kHz	2.570982	6.5
16/06/2024_1	60477.016	10 kHz	2.613878	2.6
16/06/2024_2	60477.100	10 kHz	2.613897	2.8
16/06/2024_3	60477.980	10 kHz	2.614058	2.4
17/06/2024_1	60478.062	10 kHz	2.614075	3.0
18/06/2024_1	60479.988	10 kHz	2.614484	3.7
19/06/2024_1	60480.073	10 kHz	2.614502	5.1
22/06/2024_1	60483.044	10 kHz	2.615673	2.7
22/06/2024_2	60483.129	10 kHz	2.615705	4.8

Fig. 9 depicts the rotation period determined from 8 passes at 10 kHz observed in 2024. The slow increasing of the period due to the eddy current is clearly visible.

4.4. Direct determination of the rotation angle

In this section, we seek to determine the initial angle of rotation for a given pass, i.e. the value $\theta_0 = \theta(t_0)$ where t_0 is an arbitrary initial instant, typically the first time instant of the pass. In principle, it would be sufficient to know a single θ_0 for the whole of Ajisai's life, but over long time intervals we are limited firstly by uncertainty about the rotation period and secondly by the fidelity of the $\theta(t)$ evolution model (which is certainly neither linear nor exactly exponential). That is why, for the time being, we determine one θ_0 for each pass.

To determine the initial rotation angle at the nominal initial time t_0 directly from observations (i.e. without a detailed simulation of the sequence of flashes), we start from the series of single nominal flash epochs that have then been matched with the associated mirror. The spin axis and the rotation period have been previously determined and their estimated values are available to be used in this method.

The rotation angle $\theta(t)$ is the angle, counting along the Ajisai's equator (i.e. the plan orthogonal to the spin axis), between a reference direction attached to the celestial frame ICRF and a reference direction attached to the body frame BDF. Even if the angles are not counting along the celestial equator, we keep the concept of right ascension α along the Ajisai's equator.

The rotation angle is the right ascension of the reference direction attached to Ajisai (one of the mirrors of the triplet of 0 inclination):

$$\alpha_0 = -\theta \tag{39}$$

We choose to use $-\theta$ instead of θ in order to keep θ increasing with time.

The right ascension α_N of a point of the Ajisai's surface, materialized by the normal to the sphere, is equal to the right ascension of the reference direction incremented by the longitude:

$$\alpha_N = \alpha_0 + \lambda_N = -\theta + \lambda_N \tag{40}$$

where λ_N is the longitude of the normal in the body frame, and is known in principle from the Ajisai's configuration.

In case of flash, the normal $\hat{\mathbf{N}}$ is aligned with the bisector $\hat{\mathbf{B}}$. To get the right ascension of $\hat{\mathbf{B}}$ we use its (normalized) projection $\hat{\mathbf{B}}_P$ on the Ajisai's equator:

$$\hat{\mathbf{B}}_P = \frac{\hat{\mathbf{B}} - \left(\hat{\mathbf{W}} \cdot \hat{\mathbf{B}}\right)\hat{\mathbf{W}}}{\sqrt{1 - \left(\hat{\mathbf{W}} \cdot \hat{\mathbf{B}}\right)^2}} \tag{41}$$

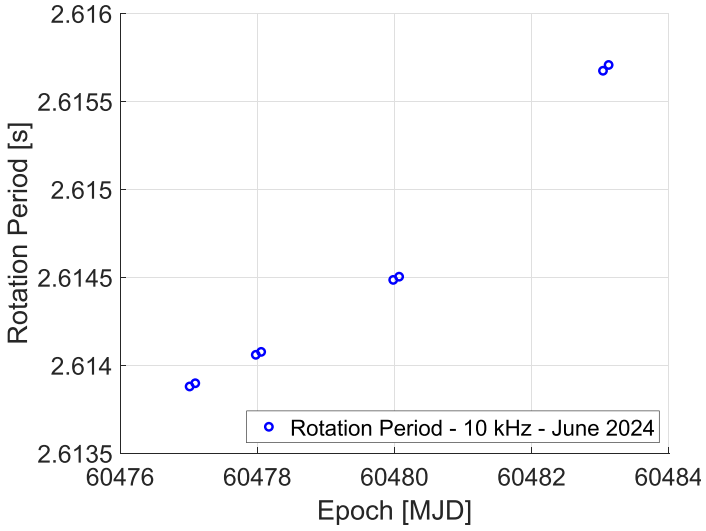

Fig. 9. Rotation period determination for 8 different passes distributed in 4 pairs. Each pair represents two successive satellite passes observed by the station during the same night.

and now we can compute its right ascension by mean of a simple scalar product with the vector $[1,0,0]^T$, i.e.:

$$\cos\alpha_B = \begin{vmatrix} x_{B_P} \\ y_{B_P} \\ z_{B_P} \end{vmatrix} \cdot \begin{vmatrix} 1 \\ 0 \\ 0 \end{vmatrix} = x_{B_P} \tag{42}$$

Since $\hat{\mathbf{N}}$ and $\hat{\mathbf{B}}$ are colinear, their right ascension are equal:

$$-\theta + \lambda_N = \alpha_B \tag{43}$$

and using the model Eq. (16) for θ, we get:

$$-\theta_0 - \dot{\theta}\cdot(t-t_0) + \lambda_N = \alpha_B. \tag{44}$$

The initial rotation angle θ_0 can thus be computed according to:

$$\theta_0 = \lambda_N - \alpha_B - \dot{\theta}\cdot(t-t_0). \tag{45}$$

Each flash, numbered k, allows to determine one value $\theta_0^{(k)}$; the value for the whole pass is computed as the mean:

$$\theta_0^{mean} = \frac{1}{N_{flashes}} \sum_{k=1}^{N_{flashes}} \theta_0^{(k)} \tag{46}$$

As previously explained, all the events must be, in principle, considered at the satellite level (epochs of reflection) rather than at the station level (epochs of reception). Fig. 10 shows an example of residuals of the individual values of the initial rotation angle w.r.t. the mean. As expected, the residuals at the reflection level are more stable than at the reception level. However, there are some values, around the middle of the window that are much larger. It is evident that they are grouped per mirror, leading to the likely assumption that this could be due to an error in the a priori longitude of the corresponding mirrors.

4.5. Comparing observations and model with determined rotation parameters

Fig. 11 depicts an example of comparison of the sequences of flashes derived, from the observations on the one hand, and from the model using the rotation parameters determined as described in the previous sections on the other hand. This is to be compared to Fig. 6 for which the model uses a priori rotation parameters. The matching is now so good that the two curves are superimposed and the points of the model hide those observed.

Fig. 12 zooms in on a shorter duration in order to clearly distinguish the successive flashes. With the a priori parameters the flashes are not emitted by the right mirrors and not at the correct instant. On the contrary, with the determined parameters, the correspondence is almost perfect.

To better evaluate the correspondence, we use the criteria M (see Eq. (23)) quantifying the matching between the presence of flashes in the sampled observations and in the model. Fig. 14 shows the values of M computed using the updated rotation parameters. Remember that M was always null when using a priori rotation parameters. With the rotation parameters determined as described above and using flat mirrors in the model, M is no longer null but never exceeds a few percents (blue bars of the figure). This is not surprising since we have evidenced that the flat mirrors model is not adequate for predicting all the observed flashes (see e.g. Fig. 4). Using the same rotation parameters but with the curved mirrors model, the matching is much better since M can reach 80% or more (red bars of the figure).

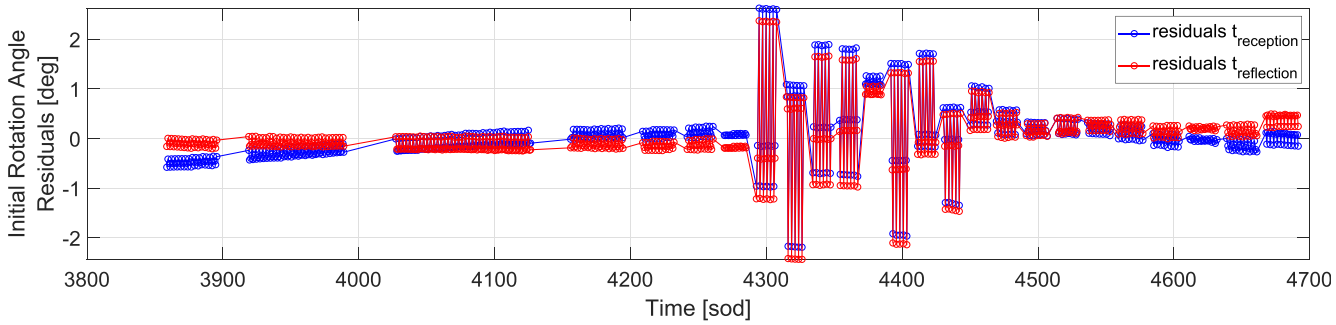

Fig. 10. Initial rotation angle residuals w.r.t. the mean. Example of a pass observed at 5 kHz on 20/04/2023.

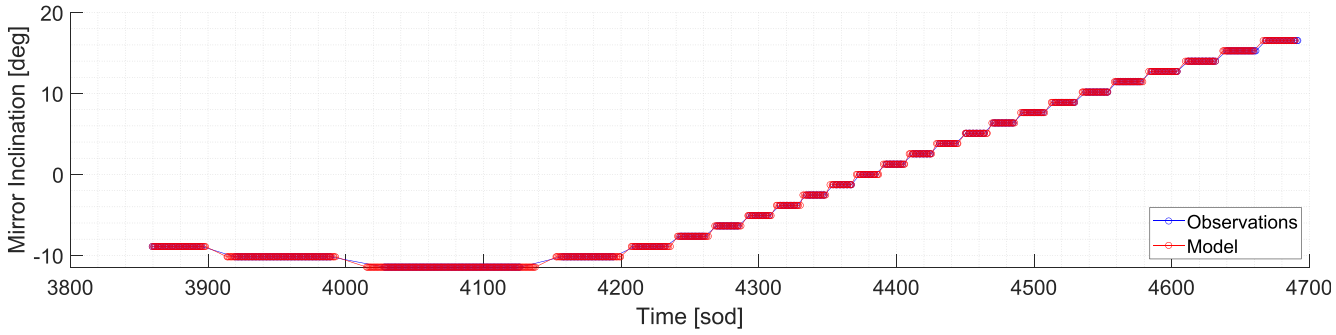

Fig. 11. Comparison of the sequences of flashes (without transitions) derived from the observations and from the model using determined rotation parameters. Observations obtained from the MéO station on 20/04/2023.

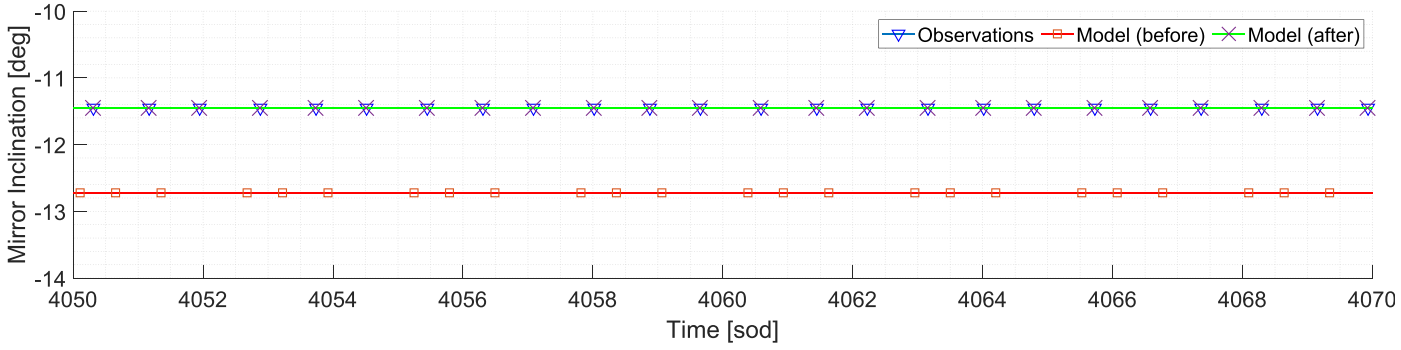

Fig. 12. Comparison of the sequences of flashes derived from the observations and from the flashes model using curved mirrors. The squares linked by the red line result from the model with a priori rotation parameters and the crosses linked by the green line result from the model evaluated using the set of rotation parameters determined by "direct method".

4.6. Global optimization of the rotation parameters through observations and model comparison

The direct method presented above is very efficient and computationally inexpensive; however it could be not optimal since it does not take into account the curvature of the mirrors and the duration of the flashes, and it implicitly considers the Sun as a point source. On the contrary, the model developed in Section 2 does not use any of these simplifying assumptions and we will use it for a global optimization of the rotation parameters. In this section, we focus on the simultaneous determination of all rotation parameters which optimizes the matching between the observations and the model. More precisely our goal is to look for the set of parameters $(\alpha^{opt}, \delta^{opt}, \theta_0^{opt}, T^{opt})$ which minimize F_{global}:

$$\min_{\alpha^{opt},\delta^{opt},\theta_0^{opt},T^{opt}} F_{\text{global}} \rightarrow \begin{cases} \alpha^{min} \leqslant \alpha^{opt} \leqslant \alpha^{max} \\ \delta^{min} \leqslant \delta^{opt} \leqslant \delta^{max} \\ \theta^{min} \leqslant \theta_0^{opt} \leqslant \theta_0^{max} \\ T^{min} \leqslant T^{opt} \leqslant T^{max} \end{cases} \tag{47}$$

where α and δ are respectively the right ascension and the declination of the spin axis, θ_0 is the initial rotation angle

and T is the rotation period. The cost function F_{global} is the number of samples for which the reflected sun light is detected in the photometry but not reproduced in the model:

$$F_{\text{global}} = \sum_{l=1}^{n_s} \left(f_l^o \cdot \left(f_l^o - f_l^m \right) \right) = n_s(1 - M) \tag{48}$$

The already precise values of the parameters found with the above direct method are used to fix the bounds of the search windows. The optimization requires to run the model a large number of times with different sets of parameters. The modification of the parameters is driven by a genetic algorithm with up to 200 generations.

The rotation parameters are not greatly modified: generally less than 1 deg. for the rotation axis and the initial rotation angle and less than 0.01 ms for the rotation period. As depicted in Fig. 14 (orange bars) the result is a further improvement in matching. However, this improvement is moderate. A possible limit could be the uncertainty on the positioning of the mirrors. Indeed, we have no formal knowledge of this positioning but have deduced it from the literature, with the risk of some margin of error. Moreover, the results of the determination of the initial rotation angle (see in particular Fig. 10) show that there is probably a source of improvement.

5. Improvement of the positioning of mirrors

We are relatively confident about the distributions of latitudes and tilts of the mirrors which are fairly regular. On the contrary, the distribution in longitude is irregular and our reconstruction from figures in the literature is necessarily imperfect. Having fixed the rotation parameters, the same optimization method can be applied to correct the longitudes of the mirrors. In principle, it could be preferable to determine the rotation parameters and the positions of all mirrors at the same time in a single global optimization, but in practice this is too cumbersome and the mirrors are considered one by one as explained below.

Here, we fixed the values of the rotation parameters according to the results of the optimization described in the previous section, and we minimize the objective function by changing the longitude λ_i of a given mirror i:

$$\min_{\lambda_i^{opt}} F_{\lambda_i} \rightarrow \left\{ \lambda_i^{min} \leqslant \lambda_i^{opt} \leqslant \lambda_i^{max} \right. \tag{49}$$

where the limits of the search window are defined as $\lambda_i \pm \Delta\lambda$ where λ_i is the initial value and with $\Delta\lambda = 1.5$ deg. The process is iterated for each of the mirrors used for the pass.

For example, for the pass observed on 16/06/2024 at 10 kHz, the longitudes of 60 mirrors have been modified with corrections less than 2.52 deg in absolute value. Since the expected main impact of the modifications of the longitudes of the mirrors relates to the initial rotation angle, we iterate the fast direct determination described in Section 4.4. As depicted in Fig. 13 the deviation of the multiple determinations of the initial rotation angle is now much lower. The residuals now range from -0.03 to $+0.03$ deg. (instead of $[-2.52; +2.25]$ before the mirrors optimization) and most of them are smaller than the 0.013 deg. of

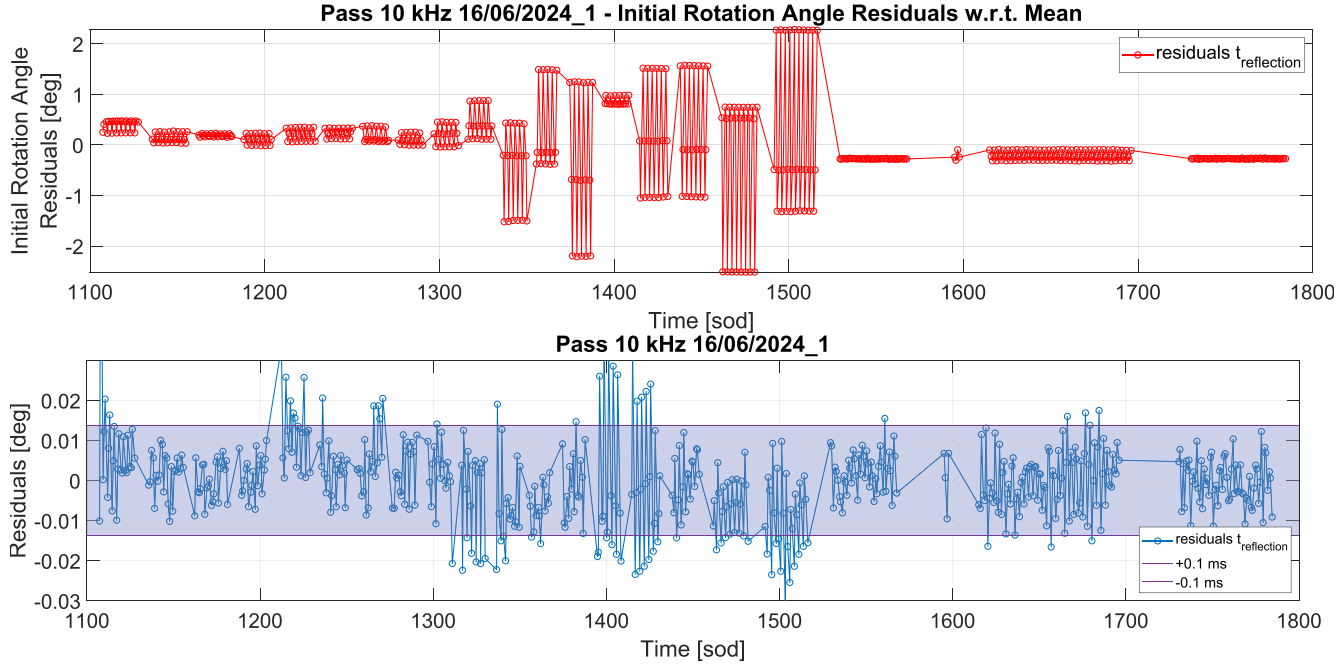

Fig. 13. Initial rotation angle residuals w.r.t. the mean obtained using the initial configuration (i.e. longitudes) of the mirrors (top panel) and with the corrected longitudes (bottom panel). Example of a pass observed at 10 kHz on 16/06/2024. The violet band delimits the displacement equivalent to the rotation in 0.1 ms which is the time sampling step for this pass.

rotation corresponding to the time sampling step of 0.1 ms. The standard deviation associated to the estimated initial rotation angle for a pass (as the mean of the values estimated from each flash) ranges from 0.5 to 1 deg. before the mirrors optimization and from 0.01 to 0.07 deg. after correction. An other favorable indicator is the significant improvement of the matching factor M (purple bars of Fig. 14) which is now close to 100% for all passes. Finally, Fig. 15 shows the comparison of the light flux computed from the model (Eq. (8)) with the observed flux. Even if this was not the goal of this paper, we note the convincing similarity, in time position, duration and shape.

To close the process, we should iterate with a global optimization looking for a new determination of the rotation parameters. We have checked that the estimates of the spin axis orientation and of the rotation period are almost not affected by the modification of the longitude of the mirrors, which is hardly surprising. But at this stage, despite the consistency of the results, a legitimate question arises: are these changes in the mirrors not merely a degree of freedom used to compensate for the limitations of the model or observations? The fact that the changes are reproducible from one pass to the next is a good indication that this is not the case. However, we only have a few passes

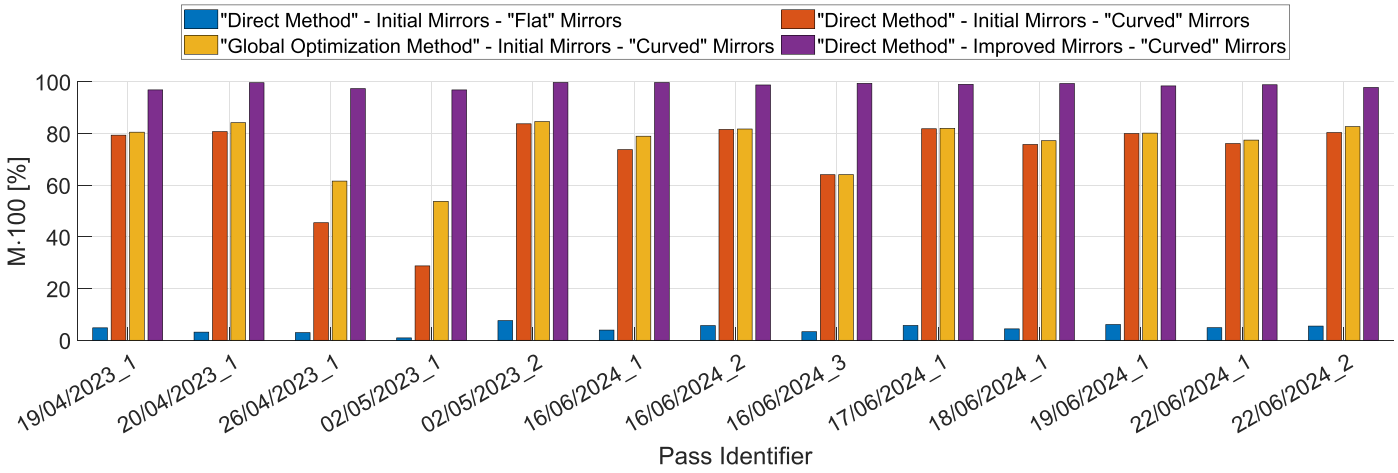

Fig. 14. Matching ratio M (see Eq. 23) for different determinations of the rotation parameters. Each test (corresponding to a color of a bar in the grouped chart) involves 3 choices of configuration: (i) the method used to determine the rotation parameters (direct or global), (ii) the positioning of the mirrors (initial or improved after optimization), and (iii) the shape of the mirrors (flat or curved) used to compute the matching ratio. Note that even if the direct method for the determination of the rotation parameters uses a unique normal per mirror (assuming implicitly a flat shape), the matching ratio can be computed afterwards either using a model with flat mirrors or a model with. curved mirrors.

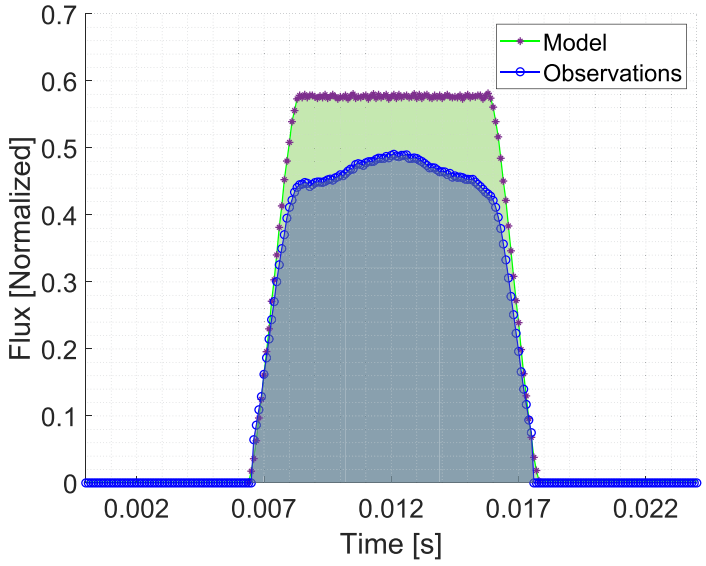

Fig. 15. Example of comparison of the observed and modeled light flux (computed from Eq. (8)) during a flash extracted from a pass observed at 10 kHz on 16/06/2024. The model uses the rotation parameters determined by the "direct method", the optimized longitude of the mirrors, and normals associated to curved mirrors discretized with a step of 0.01 deg. The comparison of the amplitudes is not relevant since both the observed and modeled flux are normalized. Nevertheless, we note that the shape and the duration of the observed flash are quite well reproduc.ed by the model.

available at the moment; more in-depth tests and stronger verifications will be carried out in the future, using more passes to fix the positioning of the mirrors once for all.

6. Conclusion

We have developed a complete model able to predict the sequences of flashes resulting from the reflection of the sunlight, by the rotating mirrors of Ajisai, towards a ground station. In particular, our model takes into account the curvature of the mirrors, that drastically changes the sequence of flashes received by the station; compared to the flat mirrors case, this increases the number of flashes leading to sequences without gaps. Moreover, this predicts transitions between triplets of mirrors, during which more than three flashes per period are generated. On the other hand, a new photometric device installed at the MéO station produced series of observed flashes for a few Ajisai's pass in 2023 and 2024. The observations are sampled at 5 kHz in 2023 and at 10 kHz in 2024. These observations confirm the better prediction of the presence of flashes when using the model with curved mirrors.

The model requires the knowledge of the attitude of Ajisai and of the configuration of the mirrors on the satellite. While we have a priori data for these quantities, we demonstrate our capacity to substantially improve the determination of the rotation parameters (the orientation of the spin axis, the rotation period, and the initial angle of rotation) from the observations. For the time being the main limit is the uncertainty on the knowledge of the configuration of the mirrors on the satellite and in particular their distribution in longitude. We have shown that we can improve significantly the correspondence between the observations and the model by slightly changing the a priori longitude of some mirrors. Although these modifications seem perfectly realistic, we will have to verify, in the future, that this can be reproduced on various independent passes. After the correction of the mirrors longitudes, the estimated precision for the determination of the rotation parameters during one pass of Ajisai are typically 0.25 deg. for the spin axis orientation, 10^{-5} s for the rotation period and 0.07 deg. for the initial rotation angle.

This work opens several exciting prospects. First we are ready to continue to observe Ajisai and to analyze the photometry in order to determine the rotation parameters on a regular basis. It would be interesting to investigate to what extent we are able to extrapolate the angle of rotation between two successive passes, i.e. over a few thousand rotations. In the medium and long term (hundreds of days) we will have to explain the evolution of the parameters with a dynamic rotation model as already done, e.g. for LAGEOS (Bertotti and Iess, 1991; Farinella et al., 1996; Métris et al., 1999; Andrés et al., 2004). There are also possibilities to study more in depth the details of the model compared to the observations: the exact consistency of the transitions, the description of single flashes (duration, shape), the detection of flashes from the CCRs. Finally, the monitoring of the rotation is an important piece of a larger project aiming to synchronize distant clocks by means of laser links on passive satellites.

Declaration of Competing Interest

The authors declare that they have no known competing financial interests or personal relationships that could have appeared to influence the work reported in this paper.

Appendix A. Differential correction of the normal to a sphere

We consider a unit vector $\hat{\mathbf{N}}$ crossing the sphere at a point P. The components of $\hat{\mathbf{N}}$ can be expressed in spherical coordinates:

$$\hat{\mathbf{N}} = \begin{bmatrix} \cos\lambda\cos\phi \\ \sin\lambda\cos\phi \\ \sin\phi \end{bmatrix} \tag{A.1}$$

where λ is the longitude counted, from an arbitrary reference direction, along the reference plane orthogonal to the polar axis $\hat{\mathbf{W}}$, and ϕ is the latitude.

A small variation of $\hat{\mathbf{N}}$ can be expanded as

$$\begin{aligned} d\hat{\mathbf{N}} &= \tfrac{d\hat{\mathbf{N}}}{d\lambda} d\lambda + \tfrac{d\hat{\mathbf{N}}}{d\phi} d\phi \\ &= \cos\phi\ \hat{\mathbf{u}}_\lambda\ d\lambda + \hat{\mathbf{u}}_\phi\ d\phi \end{aligned} \tag{A.2}$$

where

$$\hat{\mathbf{u}}_\lambda = \begin{bmatrix} -\sin\lambda \\ \cos\lambda \\ 0 \end{bmatrix} \tag{A.3}$$

is the unit vector tangent to the parallel crossing P, and

$$\hat{\mathbf{u}}_\phi = \begin{bmatrix} -\cos\lambda\sin\phi \\ -\sin\lambda\sin\phi \\ \cos\phi \end{bmatrix} \tag{A.4}$$

is the unit vector tangent to the meridian crossing P.

Conversely, since $\hat{\mathbf{u}}_\lambda$ and $\hat{\mathbf{u}}_\phi$ are orthogonal, the variations of longitude and latitude can be computed from a variation of $\hat{\mathbf{N}}$:

$$\begin{aligned} d\lambda &= \tfrac{1}{\cos\phi} d\hat{\mathbf{N}} \cdot \hat{\mathbf{u}}_\lambda \\ d\phi &= d\hat{\mathbf{N}} \cdot \hat{\mathbf{u}}_\phi \end{aligned} \tag{A.5}$$

Moreover, we have

$$\begin{aligned} \hat{\mathbf{u}}_\lambda &= \tfrac{1}{\cos\phi} \begin{bmatrix} 0 \\ 0 \\ 1 \end{bmatrix} \wedge \begin{bmatrix} \cos\lambda\cos\phi \\ \sin\lambda\cos\phi \\ \sin\phi \end{bmatrix} = \tfrac{1}{\cos\phi} \hat{\mathbf{W}} \wedge \hat{\mathbf{N}} \\ \hat{\mathbf{u}}_\phi &= \hat{\mathbf{N}} \wedge \hat{\mathbf{u}}_\lambda = \hat{\mathbf{N}} \wedge \left(\tfrac{1}{\cos\phi} \hat{\mathbf{W}} \wedge \hat{\mathbf{N}} \right) = \tfrac{1}{\cos\phi} \hat{\mathbf{W}} - \tfrac{\sin\phi}{\cos\phi} \hat{\mathbf{N}} \end{aligned} \tag{A.6}$$

Inserting in (A.5) we get

$$\begin{aligned} d\lambda &= \frac{1}{\cos^2\phi} d\hat{\mathbf{N}} \cdot \left(\hat{\mathbf{W}} \wedge \hat{\mathbf{N}}\right) \\ d\phi &= \frac{1}{\cos\phi} d\hat{\mathbf{N}} \cdot \hat{\mathbf{W}} - \frac{\sin\phi}{\cos\phi} d\hat{\mathbf{N}} \cdot \hat{\mathbf{N}} \end{aligned} \tag{A.7}$$

References

Acton, C., Bachman, N., Semenov, B., et al., 2018. A look towards the future in the handling of space science mission geometry. Planet. Space Sci. 150, 9–12. https://doi.org/10.1016/j.pss.2017.02.013.

Andrés, J.I., Noomen, R., Bianco, G., et al., 2004. Spin axis behavior of the LAGEOS satellites. J. Geophys. Res. 109 (B06403). https://doi.org/10.1029/2003JB002692.

Bertotti, B., Iess, L., 1991. The rotation of LAGEOS. J. Geophys. Res. 96 (B2), 2431–2440.

Burlak, N., Koshkin, N., Korobeynikova, E. et al. (2014). The Research of Variation of the Period and Precession of the Rotation Axis of EGS (AJISAI) Satellite by Using Photometric Measurement. Odessa Astronomical Publications, 27, 83. URL: https://ui.adsabs.harvard.edu/abs/2014OAP....27...83B. ADS Bibcode: 2014OAP....27...83B.

Charlot, P., Jacobs, C.S., Gordon, D., et al., 2020. The third realization of the International Celestial Reference Frame by very long baseline interferometry. Astron. Astrophys. 644, A159. https://doi.org/10.1051/0004-6361/202038368.

Currie, D., Kissell, K., Avizonis, P. et al., 1997. On the dynamics of the lageos-i spin vector: High precision direct observations and comparisons to theoretical modeling. In: I.M. Wytrzyszczak, J.H. Lieske, & R. A. Feldman (Eds.), Dynamics and Astrometry of Natural and Artificial Celestial Bodies (pp. 341–346). Dordrecht: Springer, Netherlands. doi:10.1007/978-94-011-5534-2_47.

Farinella, P., Vokrouhlický, D., Barlier, F., 1996. The rotation of LAGEOS and its long-term semimajor axis decay: a self-consistent solution. J. Geophys. Res. 101, 17861–17872.

Hashimoto, H., Nakamura, S., Shirai, H., et al., 2012. Japanese Geodetic Satellite AJISAI: development, observation and scientific contributions to geodesy. J. Geodetic Soc. Japan 58 (1), 9–25. https://doi.org/10.11366/sokuchi.58.9.

ILRS (2018). Consolidated Laser Target Prediction Format Version 2.0. URL:https://ilrs.gsfc.nasa.gov/docs/2018/cpf_2.00h-1.pdf.

Kirchner, G., Hausleitner, W., Cristea, E., 2007. Ajisai Spin Parameter Determination Using Graz Kilohertz Satellite Laser Ranging Data. IEEE Trans. Geosci. Remote Sens. 45 (1), 201–205. https://doi.org/10.1109/TGRS.2006.882254.

Korobeynikova, E., Koshkin, N., Shakun, S. et al. (2012). The Photometric Model of Artificial Satellite Ajisai and Determination of its Rotation Period. Odessa Astronomical Publications, 25, 216. URL: https://ui.adsabs.harvard.edu/abs/2012OAP....25.216K. ADS Bibcode: 2012OAP....25.216K.

Koshkin, N., Shakun, L., Burlak, N., et al., 2017. Ajisai spin-axis precession and rotation-period variations from photometric observations. Adv. Space Res. 60 (7), 1389–1399. https://doi.org/10.1016/j.asr.2017.06.045.

Koshkin, N.I., Korobeinikova, E.A., Strakhova, S.L., et al., 2010. Determination of the rotation parameters of reference artificial satellite AJISAI and synchronization of the photometric channels. Odessa Astronomical Publications, URL: http://dspace.onu.edu.ua:8080/handle/123456789/4799.

Kucharski, D., Kirchner, G., Otsubo, T., et al., 2020. Quanta Photogrammetry of Experimental Geodetic Satellite for remote detection of micrometeoroid and orbital debris impacts. Acta Astronaut. 174, 24–31. https://doi.org/10.1016/j.actaastro.2020.04.042.

Kucharski, D., Kirchner, G., Otsubo, T., et al., 2009. 22Years of AJISAI spin period determination from standard SLR and kHz SLR data. Adv. Space Res. 44 (5), 621–626. https://doi.org/10.1016/j.asr.2009.05.007.

Kucharski, D., Kirchner, G., Otsubo, T., et al., 2010a. The Impact of Solar Irradiance on AJISAI's Spin Period Measured by the Graz 2-kHz SLR System. IEEE Trans. Geosci. Remote Sens. 48 (3), 1629–1633. https://doi.org/10.1109/TGRS.2009.2031229.

Kucharski, D., Kirchner, G., Otsubo, T., et al., 2019. Hypertemporal photometric measurement of spaceborne mirrors specular reflectivity for Laser Time Transfer link model. Adv. Space Res. 64 (4), 957–963. https://doi.org/10.1016/j.asr.2019.05.030.

Kucharski, D., Kirchner, G., Otsubo, T., et al., 2016. Confirmation of gravitationally induced attitude drift of spinning satellite Ajisai with Graz high repetition rate SLR data. Adv. Space Res. 57 (4), 983–990. https://doi.org/10.1016/j.asr.2015.12.010.

Kucharski, D., Otsubo, T., Kirchner, G., et al., 2010b. Spin axis orientation of Ajisai determined from Graz 2kHz SLR data. Adv. Space Res. 46 (3), 251–256. https://doi.org/10.1016/j.asr.2010.03.029.

Kunimori, H., Takahashi, F., Itabe, T., 1992. Laser ranging application to time transfer using geodetic satellite and to other Japanese space programs. In: Proc. 8th International Workshop on Laser Ranging Instrumentation.

Liu, T., Eckl, J.J., Steindorfer, M. et al. (2021). Accurate ground-to-ground laser time transfer by diffuse reflections from tumbling space debris objects. Metrologia, 58(2), 025009. URL: doi: 10.1088/1681-7575/abde9e. doi:10.1088/1681-7575/abde9e. Publisher: IOP Publishing.

Mariey, H., 2022. Progress on the implementation of two-color high count rate laser ranging at Grasse. URL: https://ilrs.gsfc.nasa.gov/lw22/presentations/S08/S08-O09.Mariey_Herve.pdf.

Métris, G., Vokrouhlický, D., Ries, J., et al., 1999. LAGEOS spin axis and non-gravitational excitations of its orbit. Adv. Space Res. 23, 721–725. https://doi.org/10.1016/S0273-1177(99)00142-8.

Otsubo, T., Amagai, J., Kunimori, H., 1998. Measuring Ajisai's spin motion. In Proceedings of the 11th International Workshop on Laser Ranging. Volume 2. Deggendorf, Germany, volume 2, pp. 674–677.

Otsubo, T., Amagai, J., Kunimori, H. et al. (2000). Spin motion of the AJISAI satellite derived from spectral analysis of laser ranging data. IEEE Transactions on Geoscience and Remote Sensing, 38(3), 1417–1424. doi:10.1109/36.843036. Conference Name: IEEE Transactions on Geoscience and Remote Sensing.

Park, R.S., Folkner, W.M., Williams, J.G., et al., 2021. The JPL Planetary and Lunar Ephemerides DE440 and DE441. Astron. J. 161 (3), 105. https://doi.org/10.3847/1538-3881/abd414, URL: https://iopscience.iop.org/article/10.3847/1538-3881/abd414.

Pearlman, M.R., Noll, C.E., Pavlis, E.C., et al., 2019. The ILRS: approaching 20 years and planning for the future. J. Geodesy 93 (11), 2161–2180. https://doi.org/10.1007/s00190-019-01241-1.

Phung, D.-H., Samain, E., Chabé, J. et al. (2021). Optical bench development for laser communication OSIRIS mission at Grasse (France) station. In International Conference on Space Optics — ICSO 2020 (pp. 981–994). SPIE volume 11852. doi:10.1117/12.2599371.

Rubincam, D.P., 1988. Yarkovsky Thermal Drag on LAGEOS. J. Geophys. Res.: Solid Earth 93 (B11), 13805–13810. https://doi.org/10.1029/JB093iB11p13805, _eprint: https://onlinelibrary.wiley.com/doi/pdf/10.1029/JB093iB11p13805.

Sasaki, M., 1987. Japanese geodetic satellite for expansion of marine control. In: Proceedings International Symposium on Marine Positioning (pp. 77–85). Dordrecht: Springer, Netherlands. doi:10.1007/978-94-009-3885-4_8.

Sasaki, M., Hashimoto, H., 1987. Launch and observation program of the experimental geodetic satellite of Japan. IEEE Trans. Geosci. Remote Sens. GE-25(5), 526–533. https://doi.org/10.1109/TGRS.1987.289830.

Sengoku, A., Cheng, M.K., Schutz, B.E., 1995. Anisotropic reflection effect on satellite. Ajisai. J. Geodesy 70 (3), 140–145. https://doi.org/10.1007/BF00943689.